A Preliminary study of relationships between thermal conductivity and petrophysical parameters in Hamra Quartzites reservoir, Hassi Messaoud field (Algeria)

Ahmed Ali Zerrouki, Yves Géraud, Marc Diraison, Kamel Baddari

A Preliminary study of relationships between thermal conductivity and petrophysical parameters in Hamra Quartzites reservoir, Hassi Messaoud field (Algeria)

Ahmed Ali Zerrouki[a,*], Yves Geraud[b], Marc Diraison[c], Kamel Baddari[d]

[a] Univ Ouargla, Fac. des Hydrocarbures, des énergies Renouvelables et Sciences de la terre et de l'univers, Lab. Géologie du Sahara, 30000, Ouargla, Algeria [b] Ecole Nationale Supérieure de Géologie, CNRS UMR7359-GéoRessources, Université de Lorraine, CREGU, 2 Rue du Doyen Marcel Roubault, TSA 70605, F-54518, Vandoeuvre-lès-Nancy, cedex, France

[c] Institut de Physique du Globe de Strasbourg (IPGS), CNRS UMR7516, Université de Strasbourg, EOST, 5 Rue René Descartes, 67084, Strasbourg cedex, France [d] Laboratoire LIMOSE, Département de Physique, Faculté des Sciences, Université M'Hamed Bougara, 2 Avenue de l'indépendance, 35000, Boumerdès, Algeria

ARTICLEINFO

Keywords:
Thermal conductivity
Hamra quartzites reservoir
Petrophysical parameters
Cement
RBF neural network

ABSTRACT

In geothermic studies, the thermal conductivity (TC) is an essential parameter needed to calculate heat flow in rocks. It is obtained generally with high accuracy from laboratory measurements. The methodology proposed in this paper is to estimate the TC, which depends on many parameters; such as mineralogy, porosity, shape of voids and nature of contact between grains, based on linear and nonlinear relationships. In order to predict the thermal conductivity from other petrophysical parameters in the Hamra Quartzites reservoir, we have measured porosity, density and permeability, for dry samples taken from core wells. The correlation coefficients (R) were calculated between thermal conductivity and other petrophysical parameters for all samples. The results show that, the correlation coefficient is moderate between TC and the porosity, weak between TC, density and permeability. To improve these correlations, samples were classified into cemented and uncemented sets. A minor improvement on the correlation coefficients is noted between TC, density and porosity in uncemented samples, with values equal 0.51 and 0.73, respectively. The application of Radial Basis Function (RBF) neural networks, using density, porosity and permeability as inputs and thermal conductivity as output, permit us to predict the thermal conductivity with high precision. The correlation coefficient between TC estimated by the RBF neural network is the same as that measured in laboratory equaling 0.983.

1. Introduction

The thermal conductivity is a fundamental parameter in geothermic studies. It is an essential factor in the calculation of heat flow in fundamental and applied geothermal studies. This parameter is defined as the quantity of heat transmitted due to the unit temperature gradient (Popov et al., 1999; Lide, 1998). Divided-bar, Line-source and Optical scanning are principal laboratory techniques used to measure this parameter. The thermal conductivity of rocks is influenced by several intrinsic and extrinsic factors, such as mineralogical composition, texture, grains size, degree of crystallization, porosity, density, pressure, cracks, nature of fluid, fluid saturation, rock lamination and temperature (Jumikis, 1966; Harmathy, 1970; Fayette et al., 2000; Sevostianov, 2006; Abdulagatova et al., 2010; Alishaev et al., 2012).

The TC can be obtained by the following principal methods: (i) from empirical relationships based on laboratory measurements, which relate thermal conductivity and other petrophysical properties measurements of rocks (Özkahraman et al., 2004; El Sayed, 2011; Duchkov et al., 2014), (ii) from wells log data, by searching the major minerals composition of the rock, then derive indirectly the thermal conductivity from them (Demongodin et al., 1991; Hartmann et al., 2005, 2008) and (iii) recently some authors have used artificial intelligence to predict thermal conductivity for sandstone (Goutorbe et al., 2006; Singh et al., 2007; Vaferi et al., 2014; Gitifar et al., 2014).

Many studies are carried out to search relationships between thermal conductivity and petrophysical properties in different rock types. For example, the relationships between thermal conductivity, porosity, P and S-waves velocity in core samples of sandstone were investigated by El Sayed (2011), Haffen et al. (2013) and Esteban et al. (2015). Sukanta Roy (2014) elaborated the effect of water saturation on thermal conductivity in sedimentary rock samples and in metamorphic and igneous rocks. The relationships between thermal conductivity and other petrophysical parameters with double porosity rock characteristic were established in carbonates (Kazatchenko et al., 2006). The equations in these works have empirical forms, and are valid generally in the studied areas. If the mineralogical compositions of rock samples change in other areas, these empirical relationships yield weak results.

Radial Basis Function (RBF) neural network is a nonlinear mathematical approach. It is a particular class of multi-layer neural networks. The popularity of RBF neural networks compared to other kinds of neural networks concerns: (i) their capacity to approximate function problems, (ii) their simple and reduced architecture

(composed only of three layers), (iii) their fast convergence properties and (vi) they have no local minima problems (Kasabov, 1998). Because of these advantages, RBF neural networks were applied in

several disciplines, including in the photovoltaic process, to predict current-voltage characteristics and power-voltage (PeV) curves of a commercial PeV module (Bonanno et al., 2012), in medical diseases diagnosis (Qasem and Shamsuddin, 2011), in the identification of nuclear accidents (Gomes and Canedo Medeiros, 2015), in seismic inversions in petroleum exploration (Baddari et al., 2010), in image analysis (Cha and Kassam, 1996; Montazer and Giveki, 2015), in nanocomposite characterization of pore size measurement and wear model of a sintered CoppereTungsten (Leema et al., 2015), in the estimation of geotechnical parameters (Sinha and Wang, 2008; Mustafa et al., 2012), in geology to estimate the grade of an offshore placer gold deposit (Samanta and Bandopadhyay, 2009) and to assess rocky desertification in northwest Guangxi, China (Zhang et al., 2011).

Few studies exist that investigated for the relationships between petrophysical parameters in quartzite rocks, compared to other formations. Gupta and Sharma (2012) obtained moderate correlation coefficients between textural, petrophysical and mechanical properties for quartzite samples, taken from north-western Himalaya.

The effect of quartz on the magnetic susceptibility for quartzite rocks was investigated by Hrouda and Kapiĉka (1986). Vishnu et al. (2010) are used the anisotropy of the magnetic susceptibility to determine the magnetic foliation in quartzites and also to study the relationship between the magnetic foliation and the ultrasonic P-wave velocity. The Hamra Quartzites reservoir in Hassi Messaoud oil field is less studied compared to Cambro-Ordovician sandstone reservoirs. Benayad et al. (2013, 2014) studied the petrography and geochemistry of core samples taken from two wells in the Hamra Quartzites formation. Aïfa et al. (2014) focused their study on the relationships between magnetic susceptibility, fractures density and petrophysical parameters for core samples taken from six wells in the Hamra Quartzites reservoir.

Despite the wide application of RBF neural networks in many scientific areas and their advantages cited previously, they have not until now been applied in geothermics. In this study, the RBF neural network is used to predict the thermal conductivity, in order to reduce the laboratory measurements time; especially, in the case where the measuring is difficult, because of fractures in the samples. The RBF neural networks technique can be a good solution to estimate TC from well log measurements, or when it is difficult to obtain complete cores from drilled wells. The aim of this work is to study the petrophysical parameters obtained from laboratory measurements for dry core samples taken from the Hamra Quartzites reservoir, and to investigate relationships between thermal conductivity, porosity, density and permeability, based on the correlations between these parameters and using the RBF neural network.

2. Study area

The Hassi Messaoud oil field is situated in the southeast of Algeria (Fig. 1) and extends over 1600 km^2. It is considered the principal oil field in Algeria and it is known for wells that produce the oil from the Cambrian anisometric reservoir (Ra). The organic matter rich shale of Silurian age is the principal source rock in the Hassi Messaoud field. The drilled wells in the study area produce the oil from Cambro-
Ordovician sandstone, which is considered as the main reservoir unit. In the past, some wells produced the oil from the Hamra Quartzites reservoir by stimulation (hydraulic fracturing) and with natural fractures contribution (Askri et al., 1995; Benayad et al., 2013, 2014; Aïfa et al., 2014).

The studied core samples are taken from the Hamra Quartzites reservoir in the south-west of Hassi Messaoud oil field (depth between 3220 and 3370 m). This formation is attributed to Arenigian age (Askri et al., 1995). It is composed of moderately to well sorted, fine to coarsegrains sandstone. The quartz percentage varies from 94.90 to 99.52%, with mean of 98%. The cement is comprised mainly of quartz, clay and carbonate, with average values of 6.02%, 2.48% and 0.57%, respectively. The geochemical study of samples taken from the Hamra Quartzites reservoir in southern Hassi Messaoud shows that, all the studied samples are characterized by high silica content, which ranges between 93.28 and 98.79 wt% (Benayad et al., 2013).

3. Materials and methods

3.1. Thermal conductivity

From Fourier's law, the thermal conductivity is given by the following equation:

$$q = -\lambda \frac{dT}{dx} \quad (1)$$

where q(W.m^{-2}), $dT\,d/\,x$(K.m^{-1}) and λ(W m^{-1}.K^{-1}) are the heat flow, the temperature gradient and the thermal conductivity, respectively.

The thermal conductivity of the studied samples was measured using the optical scanning method. The principle of this method is simple; the device is a

movable block form, with two temperature sensors sensitive to the electromagnetic radiation and the heat source. They are aligned parallel to the displacement axis for allowing the measurement of the sample temperature before and after heating. This
block moves along the measuring line with a constant velocity to give the thermal conductivity profile (Popov et al., 1999).

The core samples were obtained during drilling of the pay zone of the Hamra Quartzites formation, using diamond drill bit and drilling fluids. The cores have a cylindrical form with 8 cm of diameter and a thickness that ranges between 3 and 10 cm, taken from different facies (Fig. 2). The samples are taken from wells #119, #114 and #105. The samples were dried for 72 h in an electric oven at temperature of 37 °C. The surface area of samples, which was exposed to the thermal beam, was painted black in order to ensure a uniform heat reflection. The measurements were executed at room conditions (1 atm and 22 °C) and were taken each 1 mm. The analyzed surface is determined as an arithmetic average of the local conductivity along an entire scanning line, and the relative measurement error is less than 3% (Popov et al., 1999).

3.2. Density and porosity measurements

The rock density is defined as the quotient of the mass and the volume of the material (Schön, 2011). The sedimentary rocks are constituted by solid grains, which take many shapes. Sometimes, the sedimentary rocks are cemented and may have voids between grains that are filled with fluids (Monicard, 1975). The

porosity is a fundamental petrophysical parameter in sedimentary rocks; which controls the storage capacity of fluids in reservoirs. It can be measured directly from plugs based on bulk and skeletal densities, gas expansion, displacement techniques (Schön, 2011), or indirectly in wells using; neutron, density and sonic log data. Recently, nuclear magnetic resonance method is also used to obtain the porosity (Bortolotti et al., 2006; Dillinger and Esteban, 2014; El Sayed and El Sayed, 2016). The density and the inferred porosity, so called Helium-porosity of samples were carried out using a gas Helium pycnometer of Micrometrics AccuPyc II 1340 type. The petrophysical parameters were measured from cylindrical samples with diameter of 1.8 cm and length that ranged from 2 to 3.5 cm. The measurements were repeated for each sample 5 times, and the errors found were less than 3%.

3.3. Permeability measurements

The permeability was measured for cylindrical samples using a nitrogen (N_2) gas permeameter, working at 40 bars of confining pressure. The permeameter device is composed of four parts (Fig. 3): (i) the room where the sample is placed and submitted to the confinement pressure, (ii) the head pressure transducer composed of a pressure sensor and a purge, this part allows the input pressure to be supplied to the sample, (iii) the confinement pressure transducer formed also by a pressure sensor and a purge, and (v) the bottom pressure transducer equipped with a pressure sensor, a flow meter and a tap to control the outlet pressure of the sample (Rosener, 2007; Stanek, 2013). The gas penetrates from the top of the cylindrical sample and flows out through the bottom, and then, the two pressures are recorded (Scheidegger, 1974; Debschutz et al., 1989; Géraud et al., 2010). The head pressure applied can reach 35 bars. The sample sizes are measured, and the permeability is calculated using the Darcy's law; then, it is corrected of the Klinkenberg's effect (Klinkenberg, 1941). The permeability was measured for the same samples, which were used for the density and the porosity measurements.

3.4. Microscopy analysis

After the thermal conductivity measurements, each sample was cut in two parts, the first is reserved for density, porosity and permeability measurements, and the second is reserved for thin sections preparation. The plane polarized light microscopy analysis is used to classify samples in cemented and uncemented grain sets. The first set contains 15 samples and the second includes 13 samples (Table 1).

4. Radial basis function neural networks

The idea of artificial neural networks is inspired from biological neural networks. The biological neuron is composed of three main components, which are responsible for the transmission of information (McCulloch and Pitts, 1943). Through the dendrites, the information flows from outside to the soma. Then, it is processed by the neuron and passed along the axon to be transmitted to other neurons (Fausett, 1994). After the work of McCulloch and Pitts (1943), many other types of artificial neural networks are appeared; for example, Hopfield neural networks (Hopfield, 1982), the adaptive resonance theory networks (Carpenter and Grossberg, 1987) and the self-organizing map (Kohonen, 1989).

The main differences between the different types of artificial neural networks lie in their architectures, learning paradigms (supervised, unsupervised and hybrid) and algorithms used in training. Their choice of application is linked to the complexity of the posed problem and the time necessary for data treatment. The RBF neural networks were developed by Broomhead and Lowe (1988). They are composed of three layers; the input layer connects directly the exterior environment to the network, its role is limited only to introduce input data to network neurons and it doesn't execute any calculation. The hidden layer includes nodes, which are activated by radial basis functions (usually Gaussian). Nonlinear transformation is applied from the input layer to the hidden layer. The output layer produces the final results of the artificial neural network. The activation function between the hidden layer and the output layer is linear. In RBF neural networks, only the weights connecting the hidden and the output layers can be modified during training. The radial function is symmetrical around the centre (Haykin, 1999; Rennard, 2006). The basic RBF neural network structure is shown in Fig. 4.

The output corresponding to the input for the jth hidden neuron of the RBF neural network is given by the equation:

$$y(x) = \sum_{j=0}^{M} w_j \phi_j(x) \qquad (2)$$

where y is the output corresponding to the input vector x, w_j is the weight between the jth hidden neuron and the output neuron, ϕ_j is the radial basis function of the jth hidden neuron and M is the number of neurons in the hidden layer.

The radial function generally used by RBF neural networks is Gaussian; it is given by the following equation:

$$\phi_j(x) = \exp\left(-\frac{\|x - u_j\|^2}{2\delta_j^2}\right) \qquad (3)$$

where u_j and δ_j are the centre and the spread parameters of the radial basis function of the jth hidden neuron, successively. The RBF neural network in this study is trained by the self-learning method using Matlab neural network toolbox (Demuth et al., 2009). It provides the possibility of realizing a nonlinear relationship between the inputs and the output data.

5. Results

5.1. Relationships between thermal conductivity and petrophysical parameters

The advantage of establishing the relationships between the thermal conductivity and petrophysical parameters is to find an efficient tool for predicting the thermal conductivity from other petrophysical rock parameters. It is important to be able to obtain TC from other petrophysical parameters that are easily measured in wells instead of measuring it directly, which has been impossible until now. The measured petrophysical parameters allow us to study, for the first one, the relationships

between the thermal conductivity and petrophysical parameters (density, porosity and permeability) of the Hamra Quartzites reservoir samples, in Hassi Messaoud field in south-western Algeria. The obtained results for the thermal conductivity for 28 samples taken from well cores range from 3.77 to 6.26 $Wm^{-1}k^{-1}$, with mean value and standard deviation (SD) of 5.19 and 0.65 $Wm^{-1}k^{-1}$, respectively. The porosity is low to moderate; it varies from a minimum (Min) of 1.51 to a maximum (Max) of 13.12%, with mean value and standard deviation equal 5.408 and 2.502, respectively. The permeability varies between 1.9×10^{-4} and 7.342 md, with mean value of 0.305 md and with slightly high standard deviation of 1.382 md. The density oscillates from 2.567 to 2.682 g/cm^3, its mean value and standard deviation equal 2.632 and 0.032 g/cm^3, respectively (Tables 1 and 2).

The results for all samples show a weak correlation (R = 0.27) between thermal conductivity and density (Fig. 5a). The increase in porosity decreases the thermal conductivity and the correlation coefficient between these two parameters equals 0.68 (Fig. 5b). The plot of the thermal conductivity as function of the permeability shows a weak correlation (Fig. 5c). The majority of permeability results for the studied samples don't exceed 0.481 md, which reflects the nature of the low permeability of the Hamra Quartzites reservoir, except, the sample number 28, which is characterized by a high permeability, compared to the other samples due to the fractures effect.

Fig. 6 shows thin section photomicrograph for the uncemented sample observed under plane-polarized light microscopy. The sample 25 is composed of coarse and fine grains, in which the quartz is the principal mineral. There is no cement between grains, which permit us to classify this sample as uncemented. Fig. 7 is a photomicrograph for the sample 15, taken from the cemented set. The grains of this sample are cemented and the distinction between these grains is difficult due to the nature of mineral cement composed essentially with silica.

The classification of samples in two sets (cemented and uncemented grains) shows a minor improvement of the correlation coefficients between the thermal conductivity, density and porosity in uncemented set. The correlation coefficient between TC and density show weak increases from 0.27 for all samples (Fig. 5a), to 0.51 for uncemented samples (Fig. 8b). But in cemented samples, the correlation coefficient is weak (Fig. 8a). The highest correlation coefficient is obtained between TC and the porosity for uncemented sample set (R = 0.73) (Fig. 9b), but in the cemented samples, the correlation coefficient is reduced from 0.68 (Fig. 5b) to be 0.44 (Fig. 9a). The correlation coefficient between thermal conductivity and permeability is very low for both sample sets (Fig. 10), and equals 0.10 for cemented sample set (Fig. 10a). This means that, the cementation is not an essential factor, which controls the relationship between TC and permeability for these samples.

The classification of samples into cemented and uncemented sets doesn't improve the correlation coefficients considerably between TC and other petrophysical parameters. The correlation coefficient increases slightly between TC, porosity and density in uncemented sample set. The correlation coefficient between TC and porosity is 0.68 for all samples and 0.73 for uncemented samples (Fig. 9b). Whereas, the correlation coefficient between TC and density is 0.51 for the same set (Fig. 8b). These results show that, the relationships between TC and petrophysical parameters can be related to other factors that controlling the thermal conductivity, which are cited previously in the introduction.

The statistical analysis of density, porosity and permeability data are shown in Table 2. The variation coefficient (Vc) of the density for all samples is 1.198%, suggesting that the density shows slight variation. In the case of cemented and uncemented sample sets, the variation coefficients are 1.254% and 1.144%, respectively. The variation coefficient of the porosity data decreases from 46.258% (in the case of all the samples) to 34.688% (for cemented sample set) and remains almost constant for uncemented samples (46.004%), which mean that, the cemented samples have homogeneous density. The permeability values are very low because the reservoir is tight, except in Sample 28, which is affected by cracks that directly influence the variation coefficient. The histograms in Figs. 11 and 12 show the variation of density, porosity and permeability values for cemented and uncemented sample sets, respectively.

5.2. Radial basis function neural network application

In the present study, a nonlinear relationship between thermal conductivity and the following petrophysical parameters; density, porosity and permeability was investigated, to facilitate the prediction of TC using the RBF neural network. The linear relationships obtained between TC and the petrophysical parameters, based on each parameter alone show weak correlation coefficients, with the exception of moderate correlation between the thermal conductivity and the porosity in uncemented samples (R = 0.73) (Fig. 9b). The RBF neural network is applied to predict TC using porosity, permeability and density as inputs and TC as output. The data measured in laboratory with high accuracy are divided in two databases, the first dataset contains 75% of data and was reserved for the training, and the second dataset includes 25% of data reserved for testing of the trained RBF neural network. The simulation is applied using Matlab software. The self-learning method was used to obtain the optimal number of neurons in the hidden layer. The training starts with one neuron in the hidden layer and a new neuron is added at each time, if the desired network error is not achieved. The training is repeated with each new neuron added until the desired error is obtained (Hirose et al., 1991). In this method the spread (δ) of the input data, changed manually during training to obtain the best spread, which produce the least error (Demuth et al., 2009). In order to evaluate the results with high accuracy, the Mean Relative Error (MRE), the Mean Square Error (MSE) and the correlation coefficient (R) are used as performance indicators, in the training and testing phases of the RBF neural network.

In the training, after checking various architectures by varying the intrinsic parameters of the network (neurons number and spread); and calculating at each time the RBF neural network performance criteria between the thermal conductivity values obtained by RBF neural network and TC measured in laboratory, a new neuron is added to the hidden layer and the training is repeated after each new hidden neuron added, until the MSE falls to an error goal (0.0001).

The results of training are shown in Table 3. Here, only the results for 1 to 12 neurons in the hidden layer with spread equal 0.7 are discussed. Other values of spread and neurons, which did not yield improvement in the network performance criteria, are not represented in Table 3. The increase of neurons number, more than 10, doesn't

improve network performance criteria in the test, despite their amelioration in the training. From 1 to 8 neurons in the hidden layer, the RBF neural network shows his capacity to learn, but it is unable to give good results in the test. With 9 neurons in the hidden layer, the performance criteria of the RBF are acceptable, but the best results are obtained with 10 neurons. The MRE, MSE and R equal 0.0029, 0.0873 and 0.8696, respectively. So, the network with this number of hidden neurons is chosen, because it gives good performances in both test and training phases (Table 3).

In the test phase, the network weights are saved for each time after the training, and the RBF neural network is used as a transfer function to predict thermal conductivity from the remained input data. The petrophysical parameters (porosity, density and permeability) data which didn't used in the training (25%) are introduced in the RBF neural network to generate the thermal conductivity, and the performance criteria (MRE, MSE and R) are calculated at each iteration. From

obtained results (Table 3), good performances are obtained with 10 neurons in the hidden layer despite the few input data used. The MRE, MSE and R equal 0.0691, 0.1472 and 0.9843, successively. The increase of the neurons number more than 10 decreases drastically the RBF neural network performance criteria. At 12 neurons for example, the MRE and MSE increase until 0.7267 and 42.2575, respectively, and the R decrease to 0.6117.

The plot of the relation between the thermal conductivity obtained by the RBF neural network and that measured in samples (Fig. 13), shows a high correlation coefficient (R = 0.983), which prove the capacity of the RBF neural network to predict the output with high accuracy from the input data.

6. Discussion

The relationships between the thermal conductivity and petrophysical parameters were investigated for core samples taken from the Hamra quartzites reservoir. The mineralogical composition of these core samples has been done in more details by Benayad et al. (2013, 2014). High values of the measured thermal conductivity reflect the mineralogical nature of samples that composed essentially of quartz, which is characterized by a high thermal conductivity compared to other minerals (TC of quartz, 7.7 $Wm^{-1}k^{-1}$) (Horai, 1971). The mineralogical composition of the Hamra quartzites reservoir is essentially the quartz (98%) (Benayad et al., 2014), which makes other minerals effect less important, compared to the quartz effect on the heat flow.

The measured values are in coherence with the results found in sandstone and tight sandstone reservoirs (Tutuncu et al., 1994; Sukanta Roy, 2014; Schön, 2015). The Hamra Quartzites reservoir is characterized by low values of permeability measured in laboratory; the majorities are less than 0.1 md, which permit to classify it in tight reservoirs (Rezaee et al., 2012). The high permeability value recorded for the sample number 28 is justified by the fractures effect. The thermal conductivity decreases with the increase of the porosity in the Hamra Quartzites reservoir, despite the moderate correlation coefficient (Fig. 5b). This trend already noticed in the case of different sedimentary rocks (Brigaud and Vasseur, 1989; Duchkov et al., 2014; Esteban et al., 2015). It is justified by the circulation of the heat flow in pores (air), which is characterized by low thermal conductivity (TC of air, 0.025 $Wm^{-1}K^{-1}$), compared to the TC of grains and rocks cement. The low correlation coefficients cited previously between TC and permeability, after the classification of samples into cemented and uncemented sets, is due to the very low permeability values. The Hamra Quartzites formation is considered as a tight reservoir. The TC is generally influenced by the porosity and density. The permeability hasn't any effect on the thermal conductivity. This result is proven by the low correlation coefficients calculated between these parameters. In some cases derived from the literature, linear relationships between TC and petrophysical parameters are found (Popov et al., 2003; Yaşar et al., 2008), but in other cases they are difficult (Mielke et al., 2017; Barry-Macaulay et al., 2013), because of the multiplicity of parameters intervening in TC, such as mineralogy, porosity, fluid content and rock structure (stratification, distribution, orientation, size and shape of the components) (Horai, 1971; Anand et al., 1973; Plewa, 1976).

The motivation behind the application of the RBF neural network in this study is to search nonlinear relation between the thermal conductivity and petrophysical parameters, then predict the thermal conductivity from them, because the linear relation between the thermal conductivity and petrophysical parameters gives low correlation coefficients. The RBF neural network with 10 neurons in the hidden layer proves its capacity to predict the thermal conductivity from porosity, permeability and density. The high correlation coefficient (R) found in training and test phases, between TC obtained by RBF neural network and that measured in laboratory, confirms the nonlinear relationship between the thermal conductivity and petrophysical parameters. Table 3 shows that, the increase of neurons number in the hidden layer improves the performance of RBF neural network in the training. In the test, the best performance criteria are obtained with 10 neurons in the hidden layer. When the number of hidden neurons is more than 10, the performance in the training became best, but the performance criteria in the test degraded, due to the over-fitting problem (Chen and Wang, 2007).

The methodology proposed in this study to estimate the thermal conductivity using the petrophysical parameters as inputs and the RBF neural network, which based on a nonlinear relationship, gives good results. It can contribute efficiently to minimize the time spent for obtaining thermal conductivity measurements in laboratory. On other hand, some authors mentioned that the RBF neural network disadvantage is the difficulty to find the topology adequate of the neural network (number of neurons in the hidden layer, connection type and function parameters (spread and centre) (Baddari et al., 2010). To solve this problem, several algorithms are proposed for training the RBF neural network, in order to obtain good results; for example, Orthogonal least squares (Chen et al., 1990), Regression tree (Orr et al., 2000) and Quick Propagation (Montazer et al., 2009).

7. Conclusion

On the light of this study, the low values of the permeability (less than 0.1 md) for the majority of samples confirm that the Hamra quartzites is a tight reservoir. The linear relationship between the thermal conductibility and the porosity shows a moderate correlation coefficient. The porosity increases with the decrease of the thermal conductivity, which confirms that the porosity is one of the main factors to control the thermal conductivity. A weak correlation coefficient found between the thermal conductivity, permeability and density. The grains cementation has low effect on the relationships between TC and petrophysical parameters. The correlation coefficient between TC, porosity and density increases slightly in uncemented set.

The RBF neural network proves to be a successful tool to estimate the thermal conductivity from petrophysical parameters. The high value of the correlation coefficient (R = 0.983) between the thermal conductivity measured in laboratory and that estimated by the RBF neural network, proves the nonlinear relationship between these parameters. On other hand, the prediction of the thermal conductivity with high accuracy using the RBF neural network and employing porosity, permeability and density as inputs, permits a quick estimation of this parameter, without a return to laboratory measurements, which take much time and sometimes are difficult to realize for some samples due to the existence of fractures.

Acknowledgments

We would like to thank the Algerian National Oil Company (Sonatrach) for providing the data. We want to express our gratitude to all the team of GeoRessources of Lorraine University and Strasbourg Institute for Earth Physics (IPGS) for their assistance in measurements and their team spirit. We are indebted to the reviewers and editor for their valuable comments, which helped us to revise properly and improve the quality of the paper.

Appendix A. Supplementary data

Supplementary data to this article can be found online at https:// doi.org/10.1016/j.jafrearsci.2019.01.005.

References

Abdulagatova, Z.Z., Abdulagatov, I.M., Emirov, S.N., 2010. Effect of pressure, temperature, and oil-saturation on the thermal conductivity of sandstone up to 250 MPa and 520 K. J. Petrol. Sci. Eng. 73, 141–155.

Aïfa, T., Ali Zerrouki, A., Baddari, K., Géraud, Y., 2014. Magnetic susceptibility and its relation with fractures and petrophysical parameters in the tight sand oil reservoir of Hamra quartzites,south west of the Hassi Messaoud oil field, Algeria. J. Petrol. Sci. Eng. 123, 120–137.

Alishaev, M.G., Abdulagatov, I.M., Abdulagatova, Z.Z., 2012. Effective thermal conductivity of fluid-saturated rocks Experiment and modeling. Eng. Geol. 135–136, 24–39.

Anand, J., Somerton, W.H., Gomaa, E., 1973. Predicting thermal conductivities of formations from other known properties. Soc. Petrol. Eng. 13, 267–273.

Aouimer, S., Cherrifi, R., 2008. Contribution de la phase tectonique Viséenne N0400 à la structuration du réservoir du quartzite du Hamra. In: Les 2ièmes Journées Internationales sur l'exploration et la production pétrolière en Afrique, vols. 26–28. Février, Tipaza, Algeria, pp. 1–20.

Askri, H., Belmecheri, A., Benrabah, B., Boudjema, A., Boumendjel, K., Daoudi, M., Drid, M., Ghalem, T., Docca, A.M., Ghandriche, H., Ghomari, A., Guellati, N., Khennous, M., Lounici, R., Naili, H., Takherist, D., Terkmani, M., 1995. In: Well Evaluation Conference Algeria (WEC), Published by Schlumberger, Produced by Technical Editing Services.

Baddari, K., Djarfour, N., Aïfa, T., Ferahtia, J., 2010. Acoustic impedance inversion by feedback artificial neural network. J. Petrol. Sci. Eng. 71, 106–111.

Barry-Macaulay, D., Bouazza, A., Singh, R.M., Wang, B., Ranjith, P.G., 2013. Thermal conductivity of soils and rocks from the Melbourne (Australia) region. Eng. Geol. 164, 131–138.

Benayad, S., Park, Y.S., Chaouchi, R., Kherfi, N., 2013. Unconventional resources in Algeria: appraisal result from the Hamra Quartzite reservoir. Geosci. J. 17, 313–327.

Benayad, S., Park, Y.S., Chaouchi, R., Kherfi, N., 2014. Parameters controlling the quality of the Hamra Quartzite reservoir, southern Hassi Messaoud, Algeria: insights from a petrographic, geochemical, and provenance study. Arab. J. Geosci. 7, 1541–1557.

Bonanno, F., Capizzi, G., Graditi, G., Napoli, C., Tina, G.M., 2012. A radial basis function neural network based approach for the electrical characteristics estimation of a photovoltaic module. Appl. Energy 97, 956–961.

Bortolotti, V., Gombia, M., Cernich, F., Michelozzi, E., Fantazzini, P., 2006. A study to apply nuclear magnetic resonance porosity measurements to seabed sediments. Mar. Geol. 230, 21–27.

Brigaud, F., Vasseur, G., 1989. Mineralogy, porosity and fluid control on thermal conductivity of sedimentary rocks. Geophys. J. Int. 98, 525–542.

Broomhead, D.S., Lowe, D., 1988. Multivariable functional interpolation and adaptive networks. Complex Syst. 2, 321–355.

Carpenter, G.A., Grossberg, S., 1987. A massively parallel architecture for a self-organizing neural pattern recognition machine. Comput. Vis. Graph Image Process 37, 54–115.

Cha, I., Kassam, S.A., 1996. RBFN restoration of nonlinearly degraded images. IEEE Trans. Image Process. 5, 964–975.

Chen, S., Billings, S.A., Cowan, C.F.N., Grant, P.M., 1990. Practical identification of NARMAX models using radial basis functions. Int. J. Contr. 52, 1327–1350.

Chen, K., Wang, L., 2007. Trends in Neural Computation. Springer-Verlag, Berlin Heidelberg.

Debschutz, W., Kruckel, U.S., Schopper, J.R., 1989. Effect of geostatic stress and pore pressure on the klinkenberg permeability factor and other fluid parameters. In: ISRM International Symposium, 30 August-2 September, Pau, France.

Demongodin, L., Pinoteau, B., Vasseur, G., Gable, R., 1991. Thermal conductivity and well logs: a case study in the Paris basin. Geophys. J. Int. 105, 675–691.

Demuth, H., Beale, M., Hagan, M., 2009. Neural Network Toolbox™ 6 User's Guide. The MathWorks, Inc.

Dillinger, A., Esteban, L., 2014. Experimental evaluation of reservoir quality in Mesozoic formations of the Perth Basin (Western Australia) by using a laboratory low field Nuclear Magnetic Resonance. Mar. Petrol. Geol. 57, 455–469.

Duchkov, A.D., Sokolova, L.S., Rodyakin, S.V., Chernysh, P.S., 2014. Thermal conductivity of the sedimentary-cover rocks of the West Siberian Plate in relation to their humidity and porosity. Russ. Geol. Geophys. 55, 784–792.

El Sayed, A.M.A., 2011. Thermophysical study of sandstone reservoir rocks. J. Petrol. Sci. Eng. 76, 138–147.

El Sayed, A.M.A., El Sayed, N.A., 2016. Petrophysical properties of clastic reservoirs using NMR relaxometry and mercury injection data: bahariya formation, Egypt. Int. J. Geophys. Geochem. 3, 28–32.

Esteban, L., Pimienta, L., Sarout, J., Piane, C.D., Haffen, S., Geraud, Y., Timms, N.E., 2015. Study cases of thermal conductivity prediction from P-wave velocity and porosity. Geothermics 53, 255–269.

Fausett, L.V., 1994. Fundamentals of Neural Networks, Architectures, Algorithms and Applications. Prentice-Hall, New Jersey.

Fayette, S., Smith, D.S., Smith, A., Martin, C., 2000. Influence of grain size on the thermal conductivity of tin oxide ceramics. J. Eur. Ceram. Soc. 20, 297–302.

Géraud, Y., Rosener, M., Surma, F., Place, J., Le Garzic, E., Diraison, M., 2010. Physical properties of fault zones within a granite body: example of the Soultz-sous-Forêts geothermal site. Compt. Rendus Geosci. 342, 566–574.

Gitifar, V., Abbasi, A., Setoodeh, P., Poursadegh, M., Sahebnazar, Z., Alamdari, A., 2014. Modeling and analysis of the thermal conductivities of air saturated sandstone, quartz and limestone using computational intelligence. Int. J. Therm. Sci. 83, 45–55.

Gomes, C.R., Canedo Medeiros, J.A.C., 2015. Neural network of Gaussian radial basis functions applied to the problem of identification of nuclear accidents in a PWR nuclear power plant. Ann. Nucl. Energy 77, 285–293.

Goutorbe, B., Lucazeau, F., Bonneville, A., 2006. Using neural networks to predict thermal conductivity from geophysical well logs. Geophys. J. Int. 166, 115–125.

Gupta, V., Sharma, R., 2012. Relationship between textural, petrophysical and mechanical properties of quartzites: a case study from northwestern Himalaya. Eng. Geol. 135–136, 1–9.

Haffen, S., Geraud, Y., Diraison, M., Dezayes, C., 2013. Determination of fluid-flow zones in a geothermal sandstone reservoir using thermal conductivity and temperature logs. Geothermics 46, 32–41.

Harmathy, T.Z., 1970. Thermal properties of concrete at elevated temperatures. J. Mater. 5, 47–74.

Hartmann, A., Rath, V., Clauser, C., 2005. Thermal conductivity from core and well log data. Int. J. Rock Mech. Min. Sci. 42, 1042–1055.

Hartmann, A., Pechnig, R., Clauser, C., 2008. Petrophysical analysis of regional-scale thermal properties for improved simulations of geothermal installations and basinscale heat and fluid flow. Int. J. Earth Sci. 97, 421–433.

Haykin, S., 1999. Neural Networks: A Comprehensive Foundation, second ed. Prentice Hall, New jersey.

Hirose, Y., Yamashita, K., Hijiya, S., 1991. Back-propagation algorithm which varies the number of hidden units. Neural Network. 4, 61–66.

Hopfield, J.J., 1982. Neural Networks and Physical Systems with emergent collective computational abilities. Proc. Natl. Acad. Sci. U.S.A. 79, 2554–2558.

Horai, K., 1971. Thermal conductivity of rock-forming minerals. J. Geophys. Res. 76, 1278–1308.

Hrouda, F., Kapička, A., 1986. The effect of quartz on the magnetic anisotropy of quartzite. Studia Geophys. Geod. 30, 39–45.

Jumikis, A.R., 1966. Thermal Soil Mechanics. Rutgers University Press, New Brunswick. Kasabov, N.K., 1998. Foundations of Neural Networks, Fuzzy Systems, and Knowledge Engineering. The MIT Press Cambridge, Massachusetts, London.

Kazatchenko, E., Markov, M., Mousatov, A., 2006. Simulation of acoustic velocities, electrical and thermal conductivities using unified pore-structure model of doubleporosity carbonate rocks. J. Appl. Geophys. 59, 16–35.

Klinkenberg, L.J., 1941. Permeability of Porous Media to Liquids and Gases. American Petroleum Institute, Drilling and production practice, pp. 200–213.

Kohonen, T., 1989. Self-organization and Associative Memory, third ed. Springer-Verlag, New York.

Leema, N., Radha, P., Vettivel, S.C., Khanna Nehemiah, H., 2015. Characterization, pore size measurement and wear model of a sintered Cu-W nano composite using radial basis functional neural network. Mater. Des. 68, 195–206.

Lide, D.R., 1998. CRC Handbook of Chemistry and Physics, 79th ed. CRC Press, Boca Raton.

McCulloch, W.S., Pitts, W.H., 1943. A logical calculus of the ideas immanent in nervous activity. Bull. Math. Biophys. 5, 115–133.

Mielke, P., Bär, K., Sass, I., 2017. Determining the relationship of thermal conductivity and compressional wave velocity of common rock types as a basis for reservoir characterization. J. Appl. Geophys. 140, 135–144.

Monicard, R., 1975. Cours de production, 1 Caractéristiques des roches réservoirs. Analyse des carottes, deuxième ed. Technip, Paris.

Montazer, G.A., Sabzevari, R., Ghorbani, F., 2009. Three-phase strategy for the OSD learning method in RBF neural networks. Neurocomputing 72, 1797–1802.
Montazer, G.A., Giveki, D., 2015. An improved radial basis function neural network for object image retrieval. Neurocomputing 168, 221–233.
Mustafa, M.R., Rezaur, R.B., Rahardjo, H., Isa, M.H., 2012. Prediction of pore-water pressure using radial basis function neural network. Eng. Geol. 135–136, 40–47.
Orr, M., Hallam, J., Murray, A., Leonard, T., 2000. Assessing RBF networks using delve. Int. J. Inf. Netw. Secur. 10, 397–415.
Özkahraman, H.T., Selver, R., Işik, E.C., 2004. Determination of the thermal conductivity of rock from P-wave velocity. Int. J. Rock Mech. Min. Sci. 41, 703–708.
Plewa, S., 1976. Correlation between thermal conductivity and other physical parameters of rocks. In: Geoelectric and Geothermal Studies. A. KAPG Geophysical Monograph. Akademiai Kiado, Budapest, pp. 49–52.
Popov, Y.A., Pribnow, D.F.C., Sass, J.H., Williams, C.F., Burkhardt, H., 1999. Characterization of rock thermal conductivity by high-resolution optical scanning. Geothermics 28, 253–276.
Popov, Y., Tertychnyi, V., Romushkevich, R., Korobkov, D., Pohl, J., 2003. Interrelations between thermal conductivity and other physical properties of rocks: experimental data. Pure Appl. Geophys. 160, 1137–1161.
Qasem, S.N., Shamsuddin, S.M., 2011. Radial basis function network based on time variant multi-objective particle swarm optimization for medical diseases diagnosis. Appl. Soft Comput. 11, 1427–1438.
Rennard, J.P., 2006. Réseaux de neuronaux: Une introduction Accompagnée d′un modèle Java. Vuibert, Paris.
Rezaee, R., Saeedi, A., Clennell, B., 2012. Tight gas sands permeability estimation from mercury injection capillary pressure and nuclear magnetic resonance data. J. Petrol. Sci. Eng. 88–89, 92–99.
Rosener, M., 2007. Etude pétrophysique et modélisation des effets des transferts thermiques entre roche et fluide dans le contexte géothermique de Soultz-sous-Forêts. Thesis, University of Strasbourg, Strasbourg.
Sadine, S.E., Bissati, S., Lourenco¸, W.R., 2016. The first true deserticolous species of Buthus Leach, 1815 from Algeria (Scorpiones: buthidae); Ecological and biogeographic considerations. Comptes Rendus Biol. 339, 44–49.
Samanta, B., Bandopadhyay, S., 2009. Construction of a radial basis function network using an evolutionary algorithm for grade estimation in a placer gold deposit. Comput. Geosci. 35, 1592–1602.
Scheidegger, A.E., 1974. The Physics of Flow through Porous Media, third ed. University of Toronto Press, Toronto.
Schön, J.H., 2011. Physical Properties of Rocks A Work Book, first ed. Elsevier, Amsterdam.
Schön, J.H., 2015. second ed. Physical Properties of Rocks: Fundamentals and Principles of Petrophysics, vol. 65 Elsevier, Amsterdam.
Sevostianov, I., 2006. Thermal conductivity of a material containing cracks of arbitrary shape. Int. J. Eng. Sci. 44, 513–528.
Sinha, S.K., Wang, M.C., 2008. Artificial neural network prediction models for soil compaction and permeability. Geotech. Geol. Eng. 26, 47–64.
Singh, T.N., Sinha, S., Singh, V.K., 2007. Prediction of thermal conductivity of rock through physico-mechanical properties. Build. Environ. 42, 146–155.
Soofi, A.S., Cao, L., 2002. Modelling and Forecasting Financial Data Techniques of Nonlinear Dynamics. Kluwer Academic Publishers, New York.
Stanek, M., 2013. Structural and Petrophysical Characterisation of Granite Intended for Radioactive Waste Stocking. Thesis, University of Strasbourg, Strasbourg.
Sukanta Roy, P.N., 2014. Effect of water saturation on rock thermal conductivity measurements. Tectonophysics 626, 137–143.
Tutuncu, A.N., Podio, A.L., Sharma, M.M., 1994. An experimental investigation of factors influencing compressional-and shear-wave velocities and attenuations in tight gas sandstones. Geophysics 59, 77–86.
Vaferi, B., Gitifar, V., Darvishi, P., Mowla, D., 2014. Modeling and analysis of effective thermal conductivity of sandstone at high pressure and temperature using optimal artificial neural networks. J. Petrol. Sci. Eng. 119, 69–78.
Vishnu, C.S., Mamtani, M.A., Basu, A., 2010. AMS, ultrasonic P-wave velocity and rock strength analysis in quartzites devoid of mesoscopic foliations-implications for rock mechanics studies. Tectonophysics 494, 191–200.
Yaşar, E., Erdoðan, Y., Güneyli, H., 2008. Determination of the thermal conductivity from physico-mechanical properties. Bull. Eng. Geol. Environ. 67, 219–225.
Zhang, M., Wang, K., Zhang, C., Chen, H., Liu, H., Yue, Y., Luffman, I., Xiangkun, Q., 2011. Using the radial basis function network model to assess rocky desertification in northwest Guangxi, China. Environ. Earth Sci. 62, 69–76.

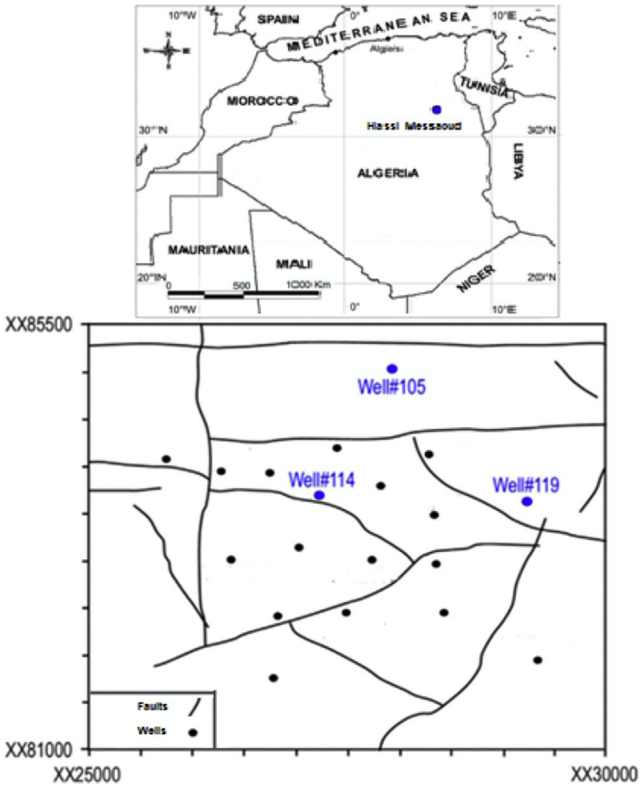

Fig. 1. Location of the study area, source (Sadine et al., 2016 and Aouimer and Cherrifi, 2008 (modified)).

Fig. 2. Photograph of core samples used for laboratory measurements before preparation.

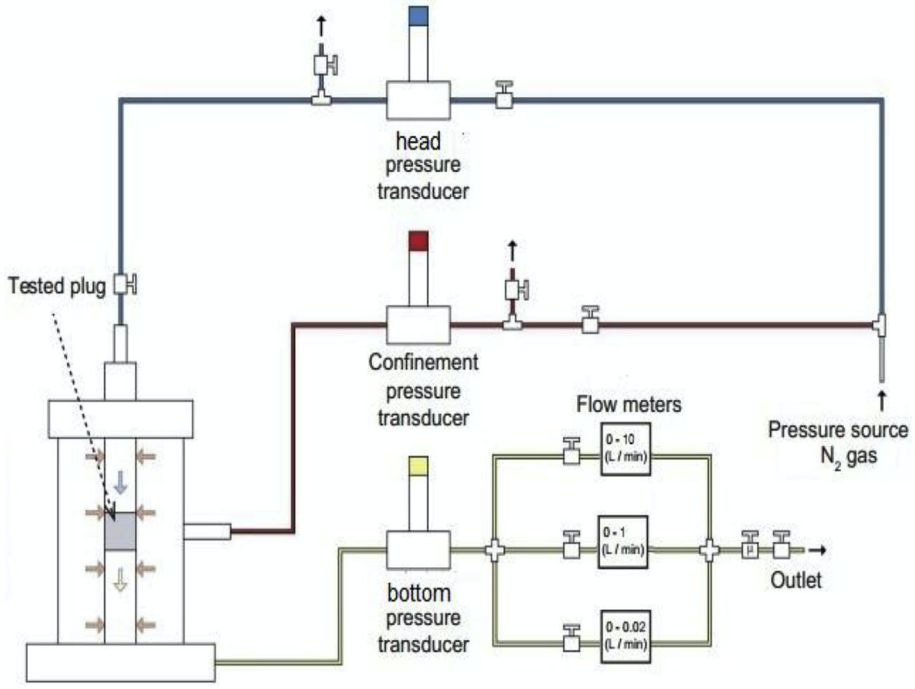

Fig. 3. A diagram showing the permeameter device using nitrogen gas flow (Rosener, 2007 and Stanek, 2013).

Table 1
Petrophysical parameters measured in laboratory for studied samples.

Sample number	Sample depth (m)	TC ($Wm^{-1}K^{-1}$)	Density (g/cm^3)	Porosity (%)	Permeability (md)	Classification in sets
W105-1	3315.83	4.82	2.67	4.59	0.021	Cemented
W114-2	3273.31	4.05	2.65	7.03	0	
W119-3	3339.70	5.29	2.62	4.33	0.048	
W114-4	3266.62	5.23	2.66	3.46	0.0057	
W105-5	3317.64	5.10	2.68	5.17	0.0062	
W114-6	3261.45	5.86	2.59	4.04	0.057	
W119-7	3334.70	5.38	2.59	3.12	0	
W119-8	3327.27	5.75	2.68	3.53	0.0014	
W119-9	3354.90	5.66	2.65	2.91	0.076	
W119-10	3352.00	4.94	2.62	7.3	0.036	
W114-11	3254.80	5.88	2.66	5.93	0.025	
W119-12	3354.90	5.65	2.64	4.61	0.003	
W114-13	3267.60	6.26	2.60	4.01	0	
W114-14	3246.00	5.25	2.61	1.51	0.00016	
W105-15	3273.31	5.41	2.59	5.53	0.18	
W105-16	3321.06	4.00	2.63	13.12	0.0075	Uncemented
W119-17	3354.90	5.66	2.66	7.38	0.035	
W119-18	3359.50	4.40	2.63	7.04	0.0088	
W105-19	3329.38	3.77	2.65	9.18	0.0061	
W114-20	3266.62	5.24	2.58	3.95	0.1256	

W114-21	3260.3	5.68	2.63	6.02	0.00019
W114-22	3261.62	5.46	2.59	6.52	0.00028
W119-23	3344.25	5.06	2.63	3.98	0.029
W114-24	3261.00	5.69	2.62	5.45	0.009
W119-25	3333.62	5.35	2.63	2.65	0.481
W114-26	3351.80	4.88	2.65	5.33	0.017
W119-27	3361.80	3.83	2.67	10.35	0.018
W119-28	3342.30	5.67	2.56	3.39	7.342

*W119-25: Means sample 25 taken from well#119.

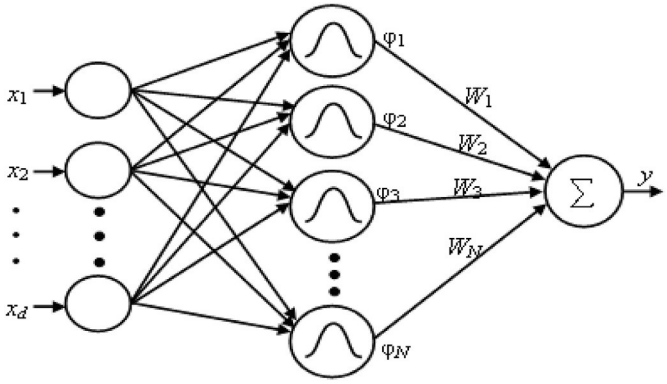

Fig. 4. The basic structure of the RBF neural network (from Soofi and Cao, 2002).

Table 2
Table showing statistical parameters of density, porosity and permeability.

	All samples			Cemented samples			Uncemented samples		
	Density (g/cm^3)	Porosity (%)	Permeability(md)	Density(g/cm^3)	Porosity (%)	Permeability(md)	Density(g/cm^3)	Porosity (%)	Permeability (md)
Min	2.567	1.510	0.00019	2.590	1.510	0	2.567	2.65	0.00019
Max	2.682	13.120	7.342	2.682	7.300	0.180	2.670	13.12	7.342
Mean	2.632	5.408	0.305	2.636	4.471	0.031	2.626	6.489	0.6215
SD	0.032	2.502	1.382	0.033	1.551	0.048	0.030	2.985	2.0235
Cv(%)	1.198	46.258	453.300	1.254	34.688	1.563	1.144	46.004	325.580

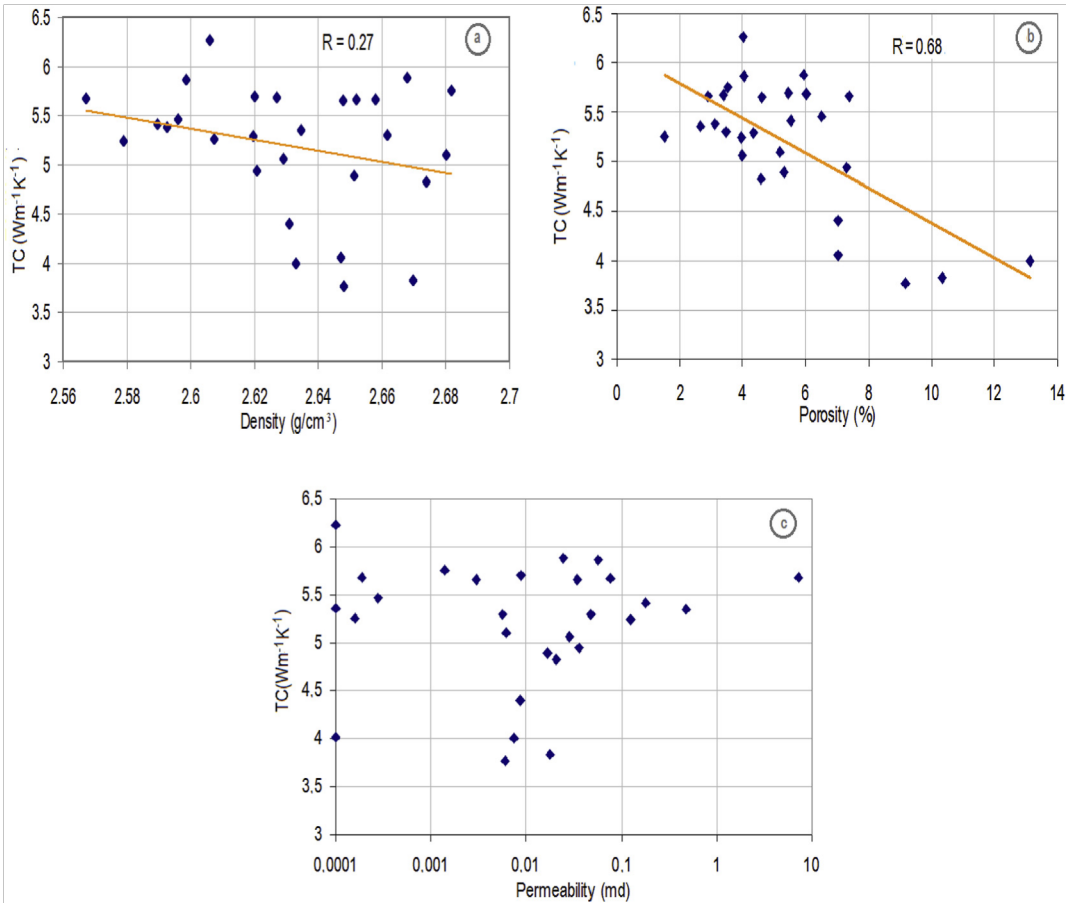

Fig. 5. A diagram showing the correlations between TC and petrophysical parameters for all samples.

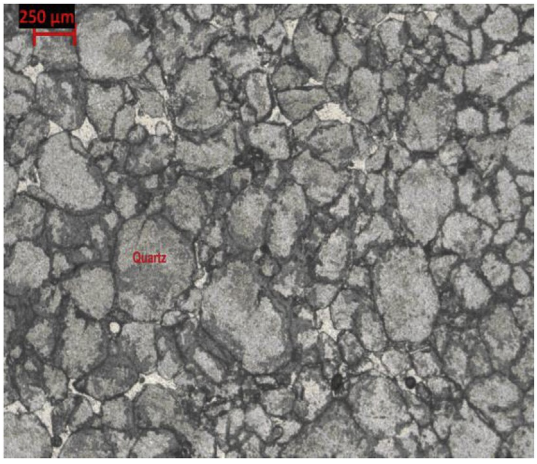

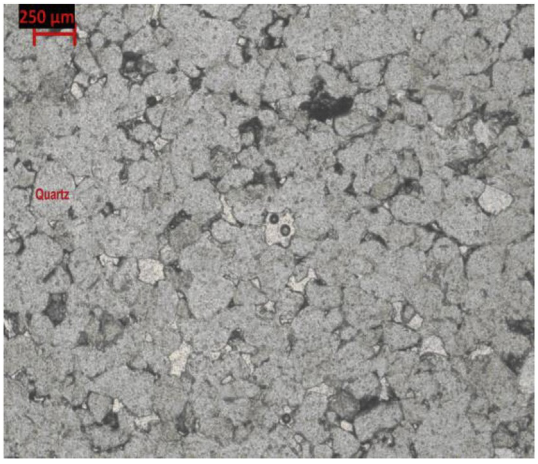

Fig. 6. Photomicrograph for sample 25 in plane polarized light showing uncemented grains.

Fig. 7. Photomicrograph for sample 15 in plane polarized light showing cemented grains.

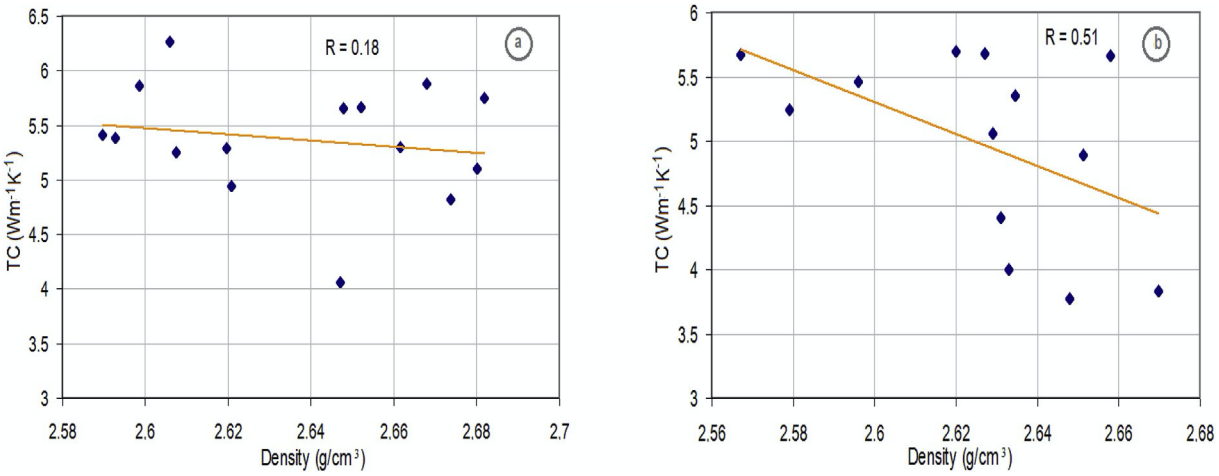

Fig. 8. Diagram showing correlation between TC and density, (a) cemented samples and (b) uncemented samples.

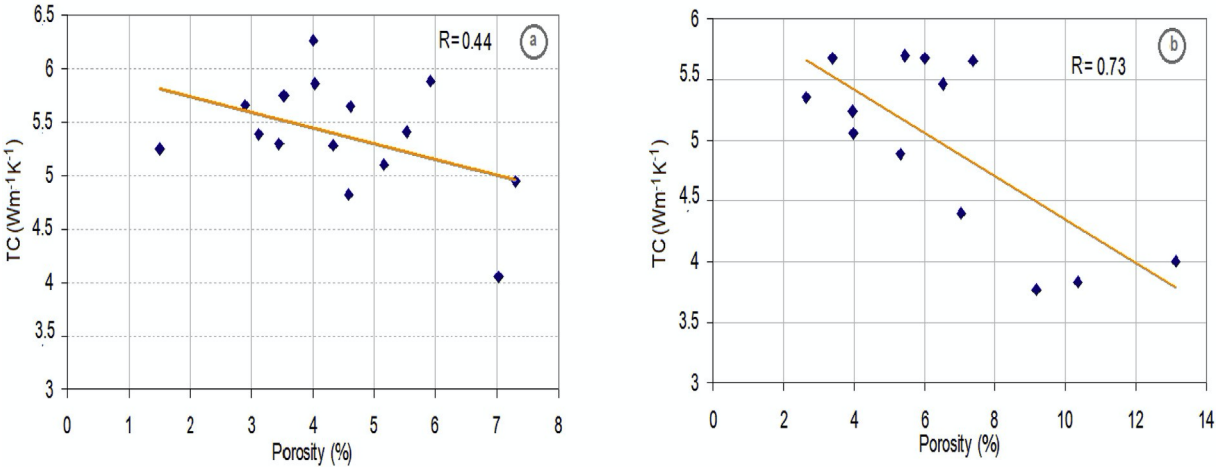

Fig. 9. Diagram showing correlation between TC and porosity, (a) cemented samples and (b) uncemented samples.

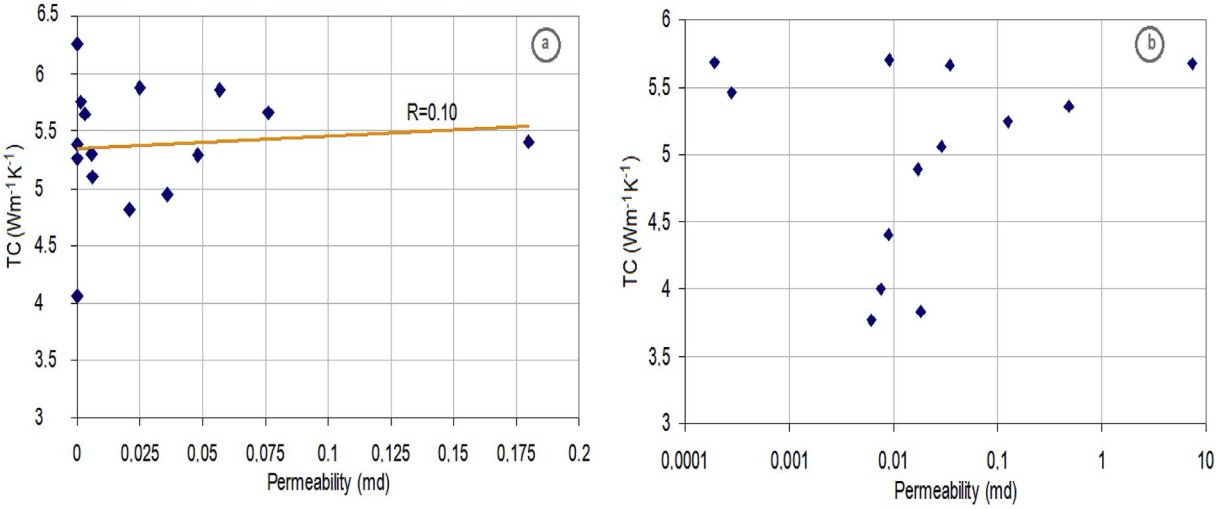

Fig. 10. Diagram showing correlation between TC and permeability, (a) cemented samples and (b) uncemented samples.

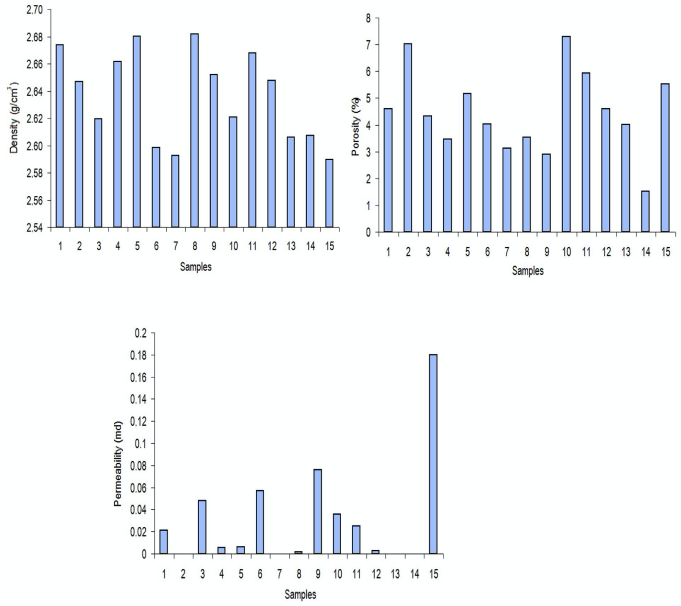

Fig. 11. Histograms of density, porosity and permeability for the cemented sample set.

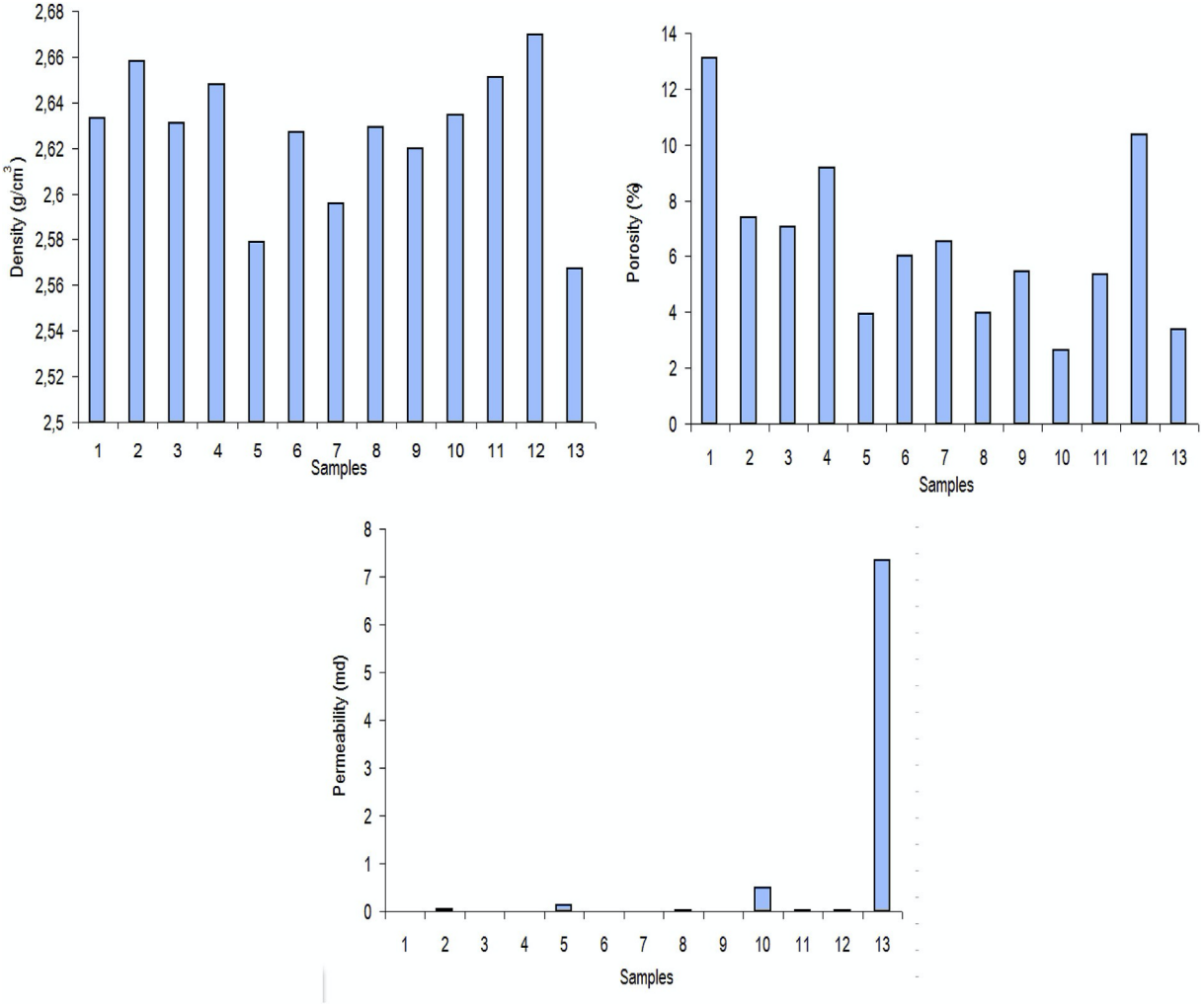

Fig. 12. Histograms of density, porosity and permeability for the uncemented sample set.

Table 3
Obtained results in the training and the testing of the RBF neural network.

Neuron numbers	Training phase			Test phase		
	MRE	MSE	R	MRE	MSE	R
01	0.0137	0.3296	0.2504	0.0594	0.5510	0.2765
02	0.0137	0.3296	0.2504	0.0597	0.5495	0.2872
03	0.0111	0.2715	0.4774	0.0660	0.4464	0.5863
04	0.0090	0.2235	0.6037	0.0597	0.3876	0.6460
05	0.0079	0.2012	0.6541	0.0530	0.3475	0.6768
06	0.0075	0.1922	0.6734	0.0583	0.3824	0.6536
07	0.0050	0.1409	0.7741	0.0720	0.5526	0.3549
08	0.0048	0.1360	0.7831	0.0838	0.5556	0.5031
09	0.0040	0.1178	0.8154	0.0693	0.1536	0.9784
10	0.0029	0.0873	0.8696	0.0691	0.1472	0.9833
11	0.0025	0.0754	0.8862	0.1266	0.5813	0.7723
12	0.0021	0.0624	0.9068	0.7267	42.2575	0.6117

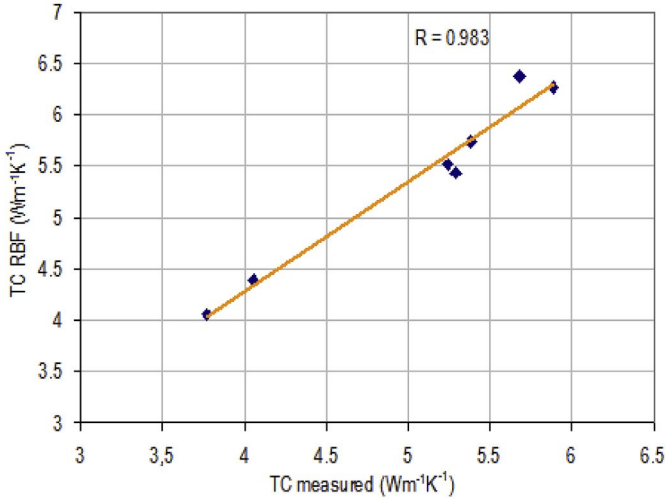

Fig. 13. Diagram showing correlation between thermal conductivity obtained by RBF neural network and that measured in laboratory.